bioRxiv preprint doi: https://doi.org/10.1101/797449; this version posted October 8, 2019. The copyright holder for this preprint (which was not certified by peer review) is the author/funder. All rights reserved. No reuse allowed without permission.

Characterization of conformational dynamics at microsecond timescale in the RNA-binding regions of dsRNA-binding domains

Harshad Paithankar,[a] and Jeetender Chugh [a,b]

[a] Department of chemistry, [b] Department of Biology, Indian Institute of Science Education & Research, Pune 411008, India.

Telephone: +91-20-25908121,

Correspondence: cjeet@iiserpune.ac.in

bioRxiv preprint doi: https://doi.org/10.1101/797449; this version posted October 8, 2019. The copyright holder for this preprint (which was not certified by peer review) is the author/funder. All rights reserved. No reuse allowed without permission.

Summary

Double-stranded RNA-binding domains (dsRBDs) are involved in a variety of biological functions via recognition and processing of dsRNAs. Though the primary substrate of the dsRBDs are dsRNAs with A-form helical geometry; they are known to interact with structurally diverse dsRNAs. Here, we have employed two model dsRBDs – TAR-RNA binding protein and Adenosine deaminase that acts on RNA – to understand the role of intrinsic protein dynamics in RNA binding. We have performed a detailed characterization of the residue-level dynamics by NMR spectroscopy for the two dsRBDs. While the dynamics profiles at the ps-ns timescale of the two dsRBDs were found to be different, a striking similarity was observed in the μs-ms timescale dynamics for both the dsRBDs. Motions at fast μs timescale (k_{ex} > 50000 s^{-1}) were found to be present not only in the RNA-binding residues but also in some allosteric residues of the dsRBDs. We propose that this intrinsic μs timescale dynamics in two distinct dsRBDs allows them to undergo conformational rearrangement that may aid dsRBDs to target substrate dsRNA from the pool of structurally different RNAs in cellular environment.

Keywords

dsRBD, dsRNA, TRBP, ADAR, conformational exchange, NMR, dynamics.

bioRxiv preprint doi: https://doi.org/10.1101/797449; this version posted October 8, 2019. The copyright holder for this preprint (which was not certified by peer review) is the author/funder. All rights reserved. No reuse allowed without permission.

Introduction

Protein-RNA interactions play a significant role in the day-to-day cellular functions. The interactions between double-stranded RNA (dsRNA) and dsRNA-binding domains (dsRBDs) are involved in complex cellular processes like RNA splicing (Fu *et al.*, 2016), RNA editing (Stephens, Haudenschild and Beal, 2004), RNA maturation (Ha and Kim, 2014), RNA transport across cellular membranes (Wang *et al.*, 2011), etc.; and hence play a central role in regulating and executing major cellular pathways governing life. Structurally, dsRBDs contain α_1-β_1-β_2-β_3-α_2 fold spanning a length of about 65-70 amino acid (Bycroft *et al.*, 1995; Kharrat *et al.*, 1995; Masliah, Barraud and Allain, 2013). Three regions of the dsRBD namely, 1) middle of helix α_1, 2) loop between β_1 and β_2, and 3) N-terminal residues of the helix α_2 are involved in the interactions with the backbone of the dsRNA at its minor-major-minor grove spanning a length of ~12 bp. Most dsRBDs are known to interact with dsRNAs having A-form helical structure independent of the sequence (Masliah, Barraud and Allain, 2013; Tants *et al.*, 2017). However, the target dsRNAs often have structural defects like internal mismatches/loops and bulges perturbing the A-form helical shape of the RNA. Such defects also lead to change in the spread of the minor-major-minor groves of the dsRNA (each represented by a unique structure defined by Euler angles (Bailor, Sun and Al-Hashimi, 2010)), thereby affecting the interaction between the dsRBD and dsRNA. Acevedo et al. have shown that interaction between dsRBD2 of TRBP does not lead to a significant conformational change in the substrate dsRNA (Acevedo *et al.*, 2016). Thus, to effectively and efficiently target a dsRNA from the wide pool of structurally different dsRNAs in the cellular matrix, dsRBDs must adapt itself to accommodate the conformational heterogeneity of the target dsRNAs.

The structural adaptations required in the proteins to perform a particular function involve conformational exchange processes characterized by motions at multiple timescales, including μs-ms timescale (Kleckner and Foster, 2011; Kamba, Nagata and Katahira, 2015; Chakrabarti *et al.*, 2017; Jie, Löhr and Barbar, 2017). These structural adaptations involve domain motions (Beach *et al.*, 2005; Kovrigin and Loria, 2006; Fraser *et al.*, 2009), catalytic interactions (Eisenmesser *et al.*, 2002; Boehr *et al.*, 2006), allosteric effects (Popovych *et al.*, 2006; Tzeng and Kalodimos, 2009), etc. Koh et al. have shown involvement of dynamics at the dsRNA-dsRBD interface where the diffusion of dsRBDs of TRBP along pre-miRNA favor its cleavage to the miRNA:miRNA* duplex by Dicer – an RNase III enzyme (Koh *et al.*, 2013). Heber et al. have recently compared binding affinities and binding stabilities of various dsRBDs in a multi-domain protein for RNA-recognition in Drosophila Staufen protein (Heber *et al.*, 2019). Fareh et al. have shown that the recognition of target dsRNA by TRBP involves

bioRxiv preprint doi: https://doi.org/10.1101/797449; this version posted October 8, 2019. The copyright holder for this preprint (which was not certified by peer review) is the author/funder. All rights reserved. No reuse allowed without permission.

dual binding modes to discriminate between the target dsRNA and other cellular dsRNAs to which protein is exposed (Fareh *et al.*, 2016).

NMR spectroscopy can provide detailed insights into such dynamic processes at an atomic resolution (Ishima and Torchia, 2000; Kempf and Loria, 2002; Loria, Berlow and Watt, 2008; Gaspari and Perczel, 2010; Kleckner and Foster, 2011). Literature available till date discusses dynamics studies by NMR spectroscopy on the dsRBDs that have been restricted to the characterization of fast (ps-ns) timescale motions in these proteins and a presence of R_{ex} calculated using model-free analysis of such motions (Nanduri *et al.*, 2000; Wostenberg, Quarles and Showalter, 2010; Wostenberg *et al.*, 2012; Hartman *et al.*, 2013). Although Chiliveri et al. have detected slow μs-ms motions (using CPMG relaxation dispersion experiments) in the α_1 helix of dsRBD1 of DRB4 protein of *A. thaliana* (Chiliveri *et al.*, 2017); they only have described R_{ex} values in their study and the detailed characterization of dynamics parameters including p_B (population of excited state), $\Delta\omega$ (chemical shift difference between ground and excited state), and k_{ex} (exchange rate between ground and excited state) remain to be performed. Apart from this study, there is no literature thus far that reports on the comprehensive characterization of μs-ms timescale dynamics in a dsRBD.

The current study attempts to characterize detailed dynamics of two model dsRBDs – namely dsRBD1 of human TAR RNA Binding Protein (TRBP2) and *Drosophila* Adenosine Deaminase Acting on RNA (dADAR) protein – at multiple timescales using NMR spectroscopy with nuclear spin relaxation and relaxation dispersion experiments. TRBP, first identified as a protein involved in an interaction with HIV TAR RNA (Gatignol *et al.*, 1991), is also known to assist Dicer (an RNase III endonuclease) to process pre-miRNAs to generate the mature microRNAs (Daniels *et al.*, 2009; Noland, Ma and Doudna, 2011; Lee and Doudna, 2012). Being a part of the canonical microRNA biogenesis pathway, TRBP is exposed to a wide array of structurally different dsRNAs. In addition to canonical α_1-β_1-β_2-β_3-α_2 secondary fold, an additional N-terminal helix α_0 was recently detected at the N terminus of dsRBD1 of TRBP2 (isoform1 of TRBP) (Masliah *et al.*, 2018; Paithankar *et al.*, 2018), the function of which remains to be understood. The second model protein used for the current investigation is the ADAR protein, known to catalyze the conversion of Adenosine to Inosine (A → I), which is critical for regulating gene expression (Bass, 2007; Barraud *et al.*, 2012; Savva, Rieder and Reenan, 2012). Human ADAR2 protein is reported to interact with dsRNAs in a sequence-specific manner (Stephens, Haudenschild and Beal, 2004; Stefl *et al.*, 2010), while *Drosophila* ADAR-dsRBD1 is reported to have less sequence-specificity (Barraud *et al.*, 2012). While both the proteins contain multiple dsRBDs, this study focusses on the dsRBD1 of these proteins to allow understanding of the intrinsic dynamics of single dsRBD (keeping any other possible domain-domain interaction aside). We observe that the two dsRBDs have a different dynamic profile at ps-ns timescale, while their dynamics profile at fast μs timescale is similar and is present not only in the RNA-binding regions but also in few allosteric residues of the dsRBDs. Being a common feature

bioRxiv preprint doi: https://doi.org/10.1101/797449; this version posted October 8, 2019. The copyright holder for this preprint (which was not certified by peer review) is the author/funder. All rights reserved. No reuse allowed without permission.

observed in two dsRBDs from two different proteins from two different species, we propose that the slow timescale motions are an intrinsic feature of the dsRBDs, that allow them to access the ensemble of conformations, required to interact with topologically different RNAs in the cellular environment.

Results

Conformational plasticity of the two dsRBDs

To investigate the conformational plasticity, if present, in the dsRBDs, CD-based melting studies were carried out. The temperature-dependent far-UV CD spectra for TRBP2-dsRBD1 showed that the protein conformation starts to open at 25°C (where all the measurements are carried out in this study) (Figure 1). The unfolding event was characterized by an enthalpy change (ΔH) of 41.11±2.32 kcal/mol and corresponding T_M of ~44°C obtained by fitting of the CD data with Gibbs-Helmholtz equation (see Methods section). The temperature-induced unfolding of dADAR-dsRBD1 using far-UV CD showed a very similar profile with enthalpy change (ΔH) of 33.58±1.57 kcal/mol and corresponding T_M of ~44°C (Figure 1). Though the thermodynamics parameters, obtained from Gibbs-Helmholtz equation, cannot be correctly interpreted due to irreversible nature of the unfolding transition (Greenfield, 2006), the melting profiles with low T_M values (similar values were obtained from the derivative plot dθ/dT vs Temperature, Figure 1E,F) hinted towards low thermal stability of the proteins at 25°C.

bioRxiv preprint doi: https://doi.org/10.1101/797449; this version posted October 8, 2019. The copyright holder for this preprint (which was not certified by peer review) is the author/funder. All rights reserved. No reuse allowed without permission.

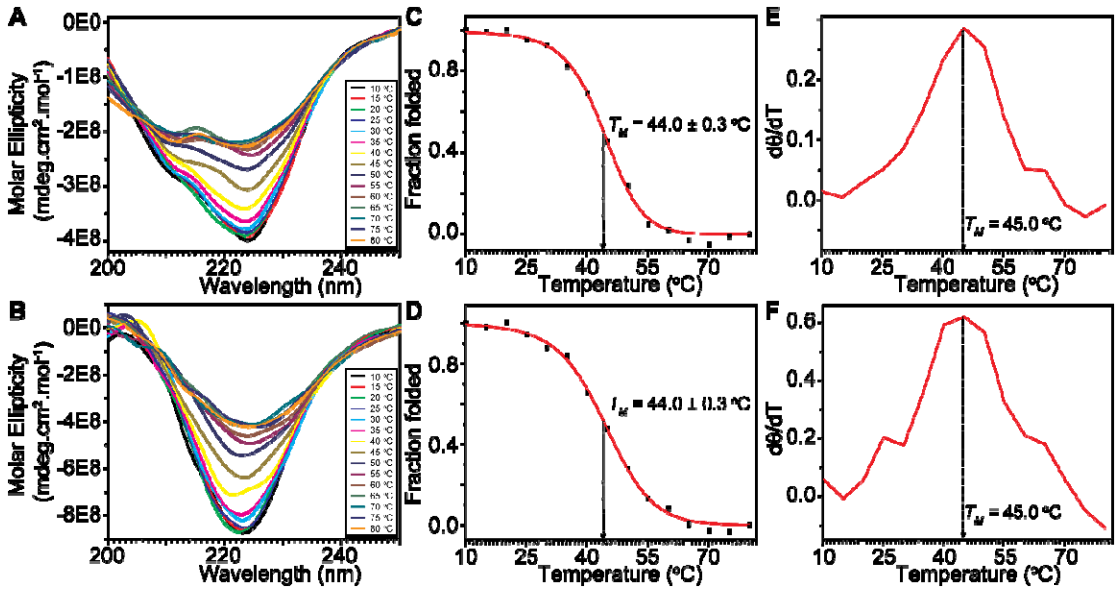

Figure 1: Conformational plasticity in dsRBDs by Circular Dichroism.
The normalized far-UV CD spectra of (**A**) TRBP2-dsRBD1 and (**B**) dADAR-dsRBD1 where molar ellipticity is plotted against wavelength measured as a function of temperature from 10 to 80 °C at an interval of 5 °C. Inset shows color scheme for the data measured at various temperatures. Fraction folded of (**C**) TRBP2-dsRBD1 and (**D**) dADAR-dsRBD1 calculated from ellipticity at 222 nm using equation 1 plotted against temperature to highlight the melting profile of the protein. First derivative plot (dθ/dT vs Temperature) of the ellipticity at 222 ns for (**E**) TRBP2-dsRBD1 and (**F**) dADAR-dsRBD1. The maxima of the curve represent the melting temperature (T_M).

TRBP2-dsRBD1 and dADAR-dsRBD1 show differential dynamics at the ps-ns timescale

To investigate the timescale of motions present in the proteins, NMR spin relaxation data (R_1, R_2 and [^{1}H]-^{15}N NOE) was analysed for 69 non-overlapping peaks out of 96 assigned peaks for TRBP2-dsRBD1 (Paithankar *et al.*, 2018) and for 58 such peaks out of 74 assigned peaks for dADAR-dsRBD1 (Barraud *et al.*, 2012) (Figure S1). The analysis of the data using the extended model-free approach (Lipari and Szabo, 1982b, 1982a; Clore *et al.*, 1990) allowed the extraction of dynamic parameters at the ps-ns timescale.

The order parameter S^2 plotted against the residue number for TRBP2-dsRBD1 have been depicted in Figure 2A,B. The theoretical values of S^2 range from 0 to 1, where 0 indicates high flexibility and 1 indicates a rigid residue (Lipari and Szabo, 1982b, 1982a). The plot showed large variations of S^2 values throughout the protein backbone. The mean S^2 for the core RNA-binding region (31-95 aa) was found to be 0.61; which suggests the presence of fast motions at ps-ns timescale in the structured regions of the protein. The residues in the α_0 helix (19-25 aa) of the protein showed higher S^2 than the N-terminal unstructured region (1-16 aa) and lower S^2 than the dsRBD core indicating the structured yet dynamic stretch of the residues in this helix. Further, the S^2 values in the stretches near the RNA-binding region showed a higher amplitude of motions compared to the overall motions of the dsRBD core. Around 78% of the analyzed

bioRxiv preprint doi: https://doi.org/10.1101/797449; this version posted October 8, 2019. The copyright holder for this preprint (which was not certified by peer review) is the author/funder. All rights reserved. No reuse allowed without permission.

residues of TRBP2-dsRBD1 showed the best fit to a 'model-free' model with motions in two timescales. The fast internal motions of the timescale of tens of picoseconds reflected random thermal motions, which were observed at the terminal and in the loop regions in the protein. Slower motions at nanosecond timescale (1-4 ns), but faster than the global tumbling time of the protein (7.64 ns), were present throughout the protein backbone.

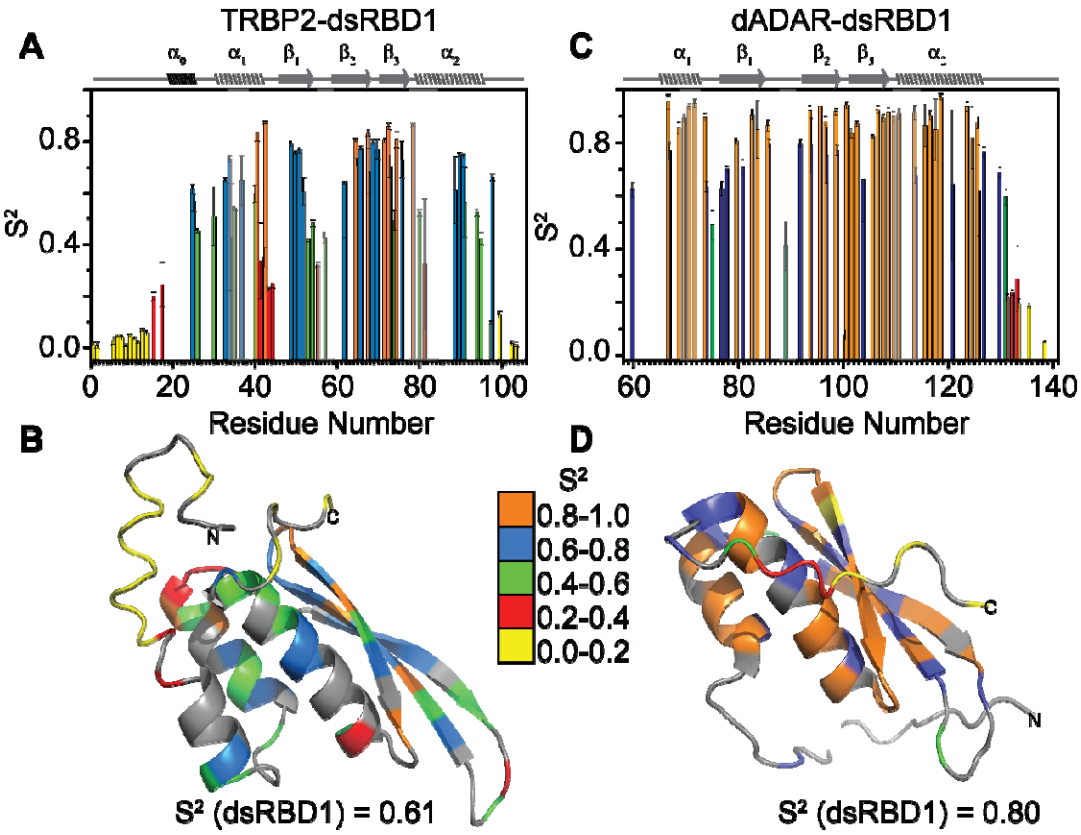

Figure 2: Differential dynamics at ps-ns timescale in the two dsRBDs.
Order parameters (S^2) calculated from the extended model-free approach plotted against residue number for (A) TRBP2-dsRBD1 and (C) dADAR-dsRBD1; S^2 values mapped in color codes on the tertiary structure of (B) TRBP2-dsRBD1 and (D) dADAR-dsRBD1. The secondary structure of the protein has been shown on the top of the section (A) and (C); and color codes for the S^2 values have been mentioned alongside section (D). Average S^2 values (excluding the N- and C-terminal flexible regions) for both the proteins have been depicted at the bottom.

The residues best fit with a model containing exchange term (R_{ex}) indicated the presence of motions at µs-ms timescale, which involved conformational exchange processes (Figure 3A). The residues having large R_{ex} were mainly observed in helix α_1 and α_2 near the RNA-binding region, and the loop regions of the protein which correlated with the lower S^2. Interestingly, a pair of residues in helix α_2 (A88 and E89) showed high S^2 values and R_{ex} at the same time.

The S^2 values calculated from model-free analysis of nuclear spin relaxation data for dADAR-dsRBD1 showed higher rigidity (when compared with that of TRBP2-dsRBD1) in the structured

bioRxiv preprint doi: https://doi.org/10.1101/797449; this version posted October 8, 2019. The copyright holder for this preprint (which was not certified by peer review) is the author/funder. All rights reserved. No reuse allowed without permission.

region of the protein with an average S^2 of 0.80 (Figure 2C,D). The only residues that showed more flexibility with lower than average S^2 value were the loop regions. The residues in the protein backbone showed motions at ns timescale (~2 ns) with fast motions at ps timescale in loop residues. Interestingly, many residues near RNA-binding region (T65, L72, E81, S82, T84, F92, I94, Q106, G107, E116, L122, R123, and S124) showed the presence of µs-ms timescale motions (similar to what was observed in TRBP2-dsRBD1) as comprehended from R_{ex} terms (Figure 3B) calculated by the extended model-free analysis. The global tumbling time for the dADAR-dsRBD1 was estimated to be a 9.39 ns from the model-free analysis.

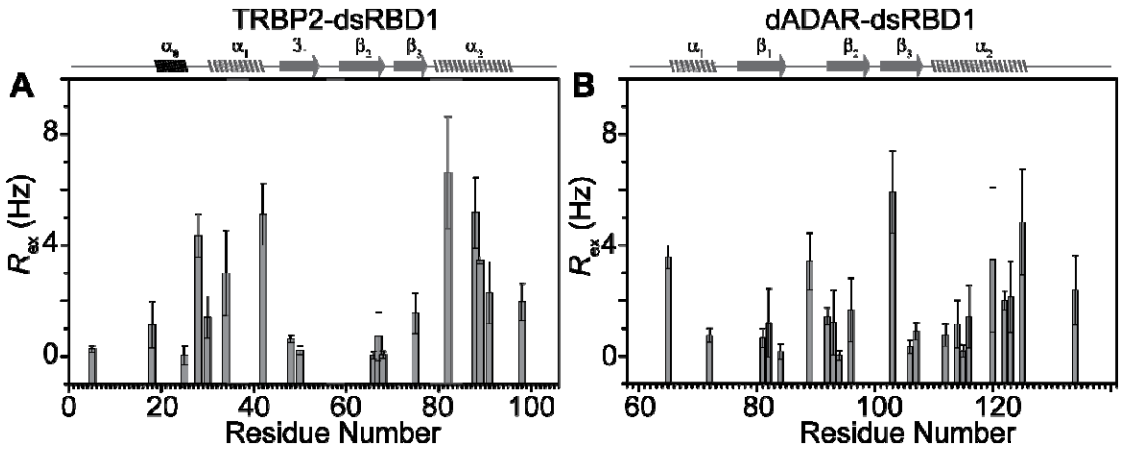

Figure 3: Slow µs-ms timescale dynamics pointed out by model-free analysis.
R_{ex} values derived from the extended model-free approach of the ^{15}N spin relaxation data (R_1, R_2 and nOe) for (A) TRBP2-dsRBD1 and (B) dADAR-dsRBD1 with secondary structure mentioned on top of plot and grey columns indicate RNA binding regions.

Conformational exchange in the µs-ms timescale in dsRBDs

Driven by the presence of R_{ex} along the length of the two dsRBDs, dynamics at µs-ms timescale was tested using Carr-Purcell-Meiboom-Gill relaxation dispersion (CPMG-RD) experiments (Loria, Berlow and Watt, 2008; Kleckner and Foster, 2011). However, R_{2eff} was found to be invariant to the CPMG frequencies (Figure S2 and Figure S3) used to create the dispersion suggesting that the dsRBDs are not conformationally exchanging at the timescale (~0.3 to 10 ms (Kleckner and Foster, 2011)) sensitive to CPMG-RD experiments. Next, dynamics at the µs-ms timescale was tested using Heteronuclear Adiabatic Relaxation Dispersion (HARD) (Mangia *et al.*, 2010; Traaseth *et al.*, 2012; Chao and Byrd, 2016) NMR experiment that monitors NMR spin relaxation in a rotating frame in the presence of hyperbolic secant (HSn, where n = stretching factor) adiabatic pulses. HARD NMR experiment allows to explore the conformational exchange processes occurring on the 10 µs to 10 ms timescales. The plot of relaxation rates $R_{1\rho}$ and $R_{2\rho}$ against residue numbers showed that as the applied field strength increases from HS1 to HS8, the $R_{1\rho}$ rates increased and the $R_{2\rho}$

bioRxiv preprint doi: https://doi.org/10.1101/797449; this version posted October 8, 2019. The copyright holder for this preprint (which was not certified by peer review) is the author/funder. All rights reserved. No reuse allowed without permission.

rates decreased for both the dsRBDs (Figure 4). The dispersion in the relaxation rates observed points to the dynamic processes that can be probed by this method. Assuming two-state exchange between a ground state and an excited state, fitting of the R_1, $R_{1\rho}$, and $R_{2\rho}$ rates to the solution of the Bloch-McConnel equations by using geometric approximation approach (Chao and Byrd, 2016) allowed to extract the residue-specific dynamic parameters (the conformational exchange rate, k_{ex}, the equilibrium populations of the two states, p_A or p_B, and the chemical shift difference, $\Delta\omega$).

Since there is a partial overlap in the timescale of motions that can be probed by CPMG-RD and HARD NMR experiments, we simulated the R_{2eff} rates for CPMG relaxation dispersion using the dynamics parameters obtained from HARD NMR experiments to verify the absence of dispersion in R_{2eff} rates as observed in CPMG-RD. The simulations for R_{2eff} values for CPMG relaxation dispersion experiment were performed using the following equation (Kleckner and Foster, 2011):

$$\boldsymbol{R_{2eff}} = R_2^0 + \frac{\Phi}{\boldsymbol{k_{ex}}}\left[1 - \frac{4\vartheta_{CPMG}}{k_{ex}}\tanh\left(\frac{k_{ex}}{4\vartheta_{CPMG}}\right)\right] \qquad (6)$$

where, $\Phi = p_A * p_B * \Delta\omega^2$ with p_A, p_B, $\Delta\omega$, and k_{ex} values used in simulation were obtained from HARD NMR data analysis. υ_{CPMG} is varied in the simulations as per the range used to record CPMG-RD data.

The simulation of the R_{2eff} rates for CPMG relaxation dispersion with equation 6 with the dynamics parameters extracted from HARD data showed no dispersion in the R_{2eff} relaxation rates.

bioRxiv preprint doi: https://doi.org/10.1101/797449; this version posted October 8, 2019. The copyright holder for this preprint (which was not certified by peer review) is the author/funder. All rights reserved. No reuse allowed without permission.

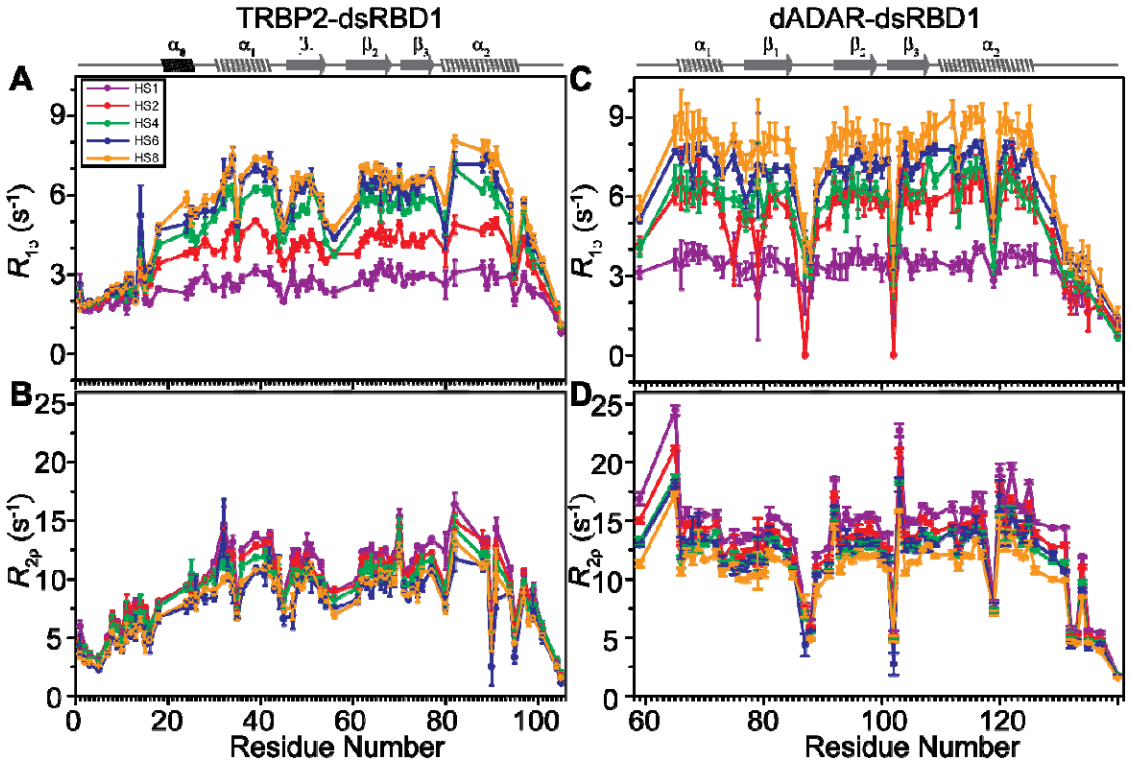

Figure 4: Dispersion in relaxation rates for two dsRBDs.
(A) $R_{1\rho}$ and (B) $R_{2\rho}$ relaxation rates derived from the adiabatic relaxation dispersion experiments plotted against residue number as a function of adiabatic pulse stretching factors (color coded for n=1,2,4,6, and 8) for TRBP2-dsRBD1. (C) $R_{1\rho}$ and (D) $R_{2\rho}$ relaxation rates from the adiabatic relaxation dispersion experiments plotted for dADAR-dsRBD1.

Careful analysis of the k_{ex} and the p_B values for TRBP2-dsRBD1, depicted on the protein structure (Figure 5A), showed that the residues in the core RNA-binding region exhibited large k_{ex} (>50000 s^{-1}) with a large excited-state population (Figure S4). The L35 and Q36 residues (lie in the middle of the α_1), the residue E54 (in the β_1-β_2 loop), and the residue A82 (lies towards the N-terminal of the helix α_2) displayed large k_{ex} values. A few of the non RNA-binding residues (A25, N26, N61, F64, T67, and V68 – although not directly interacting with dsRNA, but are present in purlieu of RNA-binding residues) also showed k_{ex} > 50000 s^{-1}. The observed exchange in these residues might have originated to maintain the overall tertiary fold of the protein during the conformational exchange happening in the RNA-binding residues. The residues in the middle of β strands, which are involved in maintaining the tertiary structure of the protein through a network of interactions (hydrophobic interactions or charge-charge interactions or H-bonding interaction) and the residues in loop/terminal regions displayed a conformational exchange occurring at the rate of 50000 s^{-1}> k_{ex} >8000 s^{-1}. These residues included (M1, T10, G13, C14, L51, V66, C73, H94, L95, A104) and about 10-40% of the population of these residues existed in excited states. Rest of the residues showed populations of <10% and are exchanging at rates <5000 s^{-1}. Along with the wide range of k_{ex} and the p_B values, wide dispersion (5-1100 Hz) in the corresponding $\Delta\omega$ values (between

bioRxiv preprint doi: https://doi.org/10.1101/797449; this version posted October 8, 2019. The copyright holder for this preprint (which was not certified by peer review) is the author/funder. All rights reserved. No reuse allowed without permission.

ground state and excited state) in ^{15}N indicated the availability of a large conformational space which the protein may populate allowing target dsRNAs to select a conformation for efficient binding (Figure S4).

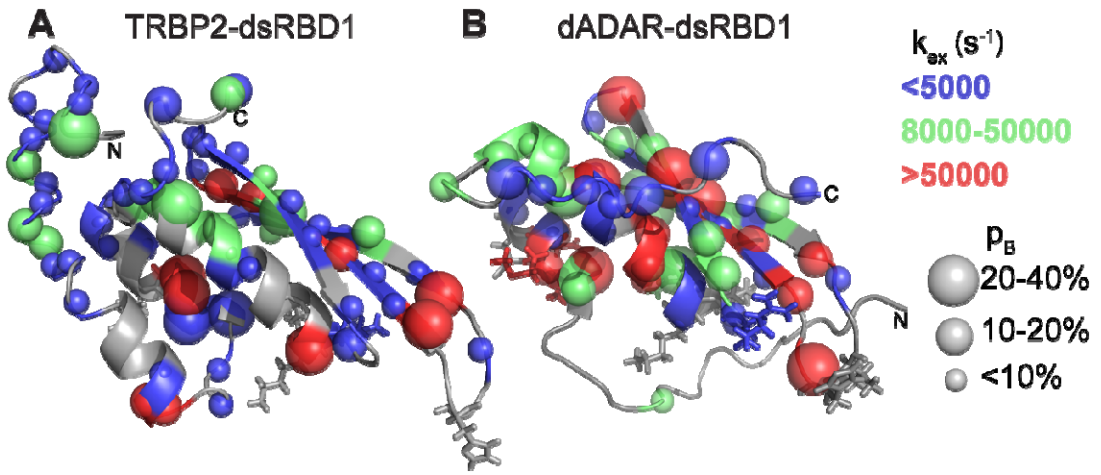

Figure 5: Conformational exchange along the backbone of the two dsRBDs.
Mapping of dynamics parameters, rate of exchange between ground state and excited state (k_{ex}), and population of the excited state (p_B) as obtained by the 'geometric approximation method' from HARD experiment, on the tertiary structure of (A) TRBP2-dsRBD1 and (B) dADAR-dsRBD1. The color code has been used to highlight the distribution of k_{ex} values whereas the size of the sphere highlights the variation in the p_B values across protein backbone. The RNA binding residues have been shown in stick mode.

Despite differences in the primary sequence of the two dsRBDs, a strikingly similar behaviour of k_{ex} was observed in dADAR-dsRBD1 (Figure 5 and Figure S4). Residues lying in the core RNA-binding region of the dsRBD, including residues in the middle of α_1 (V66, A67, M68, N70), residues in β_1-β_2 loop (T84, A89, L91), and residues towards N-terminal of α_2 (R114, I115, E116, A117) were all found to have k_{ex} > 50000 s^{-1}. Similar to TRBP2-dsRBD1, a few of the non-RNA binding residues (L76, T93, I94, S95, V96, Q101, and L104) also showed k_{ex} > 50000 s^{-1} in the region suggesting allosteric role (L76, I94, and L104 directly interact with RNA-binding residues) for the proposed conformational adaptation by dsRBD. Other residues in the non-RNA-binding region had k_{ex} between 8000 s^{-1} to 50000 s^{-1} and were found to lie in either loops or in the middle of β strands and the fraying end of helix α_2. Rest of the residues showed populations of <10% and are exchanging at rates <5000 s^{-1}. A similar chemical shift dispersion was observed in the $\Delta\omega$ values in ^{15}N for dADAR-dsRBD1 (Figure S4) as observed for TRBP2-dsRBD1.

Discussion

In order to understand the role of protein dynamics in interaction with the topologically broad range of dsRNAs, two dsRBDs – TRBP2-dsRBD1 and dADAR-dsRBD1 – were tested for the

bioRxiv preprint doi: https://doi.org/10.1101/797449; this version posted October 8, 2019. The copyright holder for this preprint (which was not certified by peer review) is the author/funder. All rights reserved. No reuse allowed without permission.

presence of dynamics. The sequence identity between the two dsRBDs was found to be 33.3% and the similarity of 23.6% with the canonical tertiary fold common to all dsRBDs. Despite the large differences in the primary sequence, both the proteins showed similar overall flexibility as evidenced by the similar CD melting profile with a T_M of ~44°C (Figure 1). Fraction-folded, as calculated from the CD data for TRBP2-dsRBD1 and dADAR-dsRBD1, showed that ~95% of the population of the dsRBDs exist in folded state at 25 °C, where all NMR experiments are recorded, suggesting presence of large conformational entropy.

Interestingly, the analysis of nuclear spin relaxation experiment by extended model-free approach showed lower order parameter values (S^2<0.6) in the structured region of the protein in addition to the low values in the loop and terminal areas for TRBP2-dsRBD1. This supported the internal flexibility in an otherwise globular protein. Order parameters for dADAR-dsRBD1, however, showed routinely observed profile with lower values (S^2<0.4) in the loop and terminal regions and higher values (S^2>0.8) in the structured regions of the protein. The global tumbling time for the two proteins as calculated from the model-free analysis was higher (7.64 ns for TRBP2-dsRBD1 and 9.39 ns for dADAR-dsRBD1) than that observed routinely for a ~11-12 kDa protein. A higher global rotational correlation time is attributed to the presence of conformational heterogeneity, the presence of an oligomeric species, and the presence of large amount of unstructured regions in the two proteins. The presence of an oligomeric species affecting the correlation time is ruled out by size-exclusion chromatography coupled with multiple angle light scattering study of the proteins. While dADAR-dsRBD1 (rotational correlation time of 9.39 s) showed a pure monomeric species, TRBP2-dsRBD1 (rotational correlation time of 7.64 ns) showed only a minor population of tetramer (Figure S5). Secondary structure analysis of the TRBP2-dsRBD1 shows that it has 45% residues in the unstructured and 55% residues in the structured regions. A similar analysis showed 59% residues in unstructured and 41% residues in structured regions of dADAR-dsRBD1. Thus, the presence of unstructured regions in the two dsRBDs could be one of the reasons for relatively higher correlation times. The presence of slow motions at µs-ms timescale suggested by model-free analysis is further tested using heteronuclear adiabatic relaxation dispersion experiment.

Analysis of HARD NMR data showed large dispersion profiles in both $R_{1\rho}$ and $R_{2\rho}$ rates when measured as a function of adiabatic pulse stretching factor, suggesting the presence of slow-dynamics at µs-ms timescale (Figure 4). The presence of strikingly similar dispersion profile in relaxation rates in both the dsRBDs indicated parallel dynamics at µs-ms timescale. Residues in the core RNA-binding region were found to have k_{ex} > 50000 s^{-1} to excited state(s) and are characterized by a large change in ^{15}N chemical shift values ($\Delta\omega$) and significant populations in excited state(s) (Figure 5 and Figure S4). Significant excited state population with a dispersion of values of $\Delta\omega$ from 5-1100 Hz is suggestive of large conformational entropy present in the dsRBDs. In addition to the faster µs timescale motions in the RNA-

bioRxiv preprint doi: https://doi.org/10.1101/797449; this version posted October 8, 2019. The copyright holder for this preprint (which was not certified by peer review) is the author/funder. All rights reserved. No reuse allowed without permission.

binding regions, conformational exchange with slower exchange rates (k_{ex} < 5000 s^{-1}) was found all along the protein backbone in both the proteins, suggesting a possibility of conformational rearrangement all along the protein chain. Although CD probed equilibrium unfolding/folding ratio as a function of temperature, and HARD relaxation dispersion experiments measured dynamics in a tight window of μs-ms timescale motions, intriguingly, they both pointed toward the presence of conformational entropy in both the dsRBDs in the experimental conditions used. Interestingly, despite the significant differences in the primary sequence of the two dsRBDs, the motions at μs-ms timescale are highly similar in RNA-binding residues and in a few allosteric regions. This suggests that the analogous dynamics observed by relaxation dispersion method in two dsRBDs are not affected by primary sequence and are intrinsic to the protein's secondary/tertiary structure. Additionally, higher k_{ex} values observed in non-RNA-binding regions manifests in the allosteric role being played by these residues to maintain the structural integrity in the conformational exchange process (Figure 5 and Figure S4). Since the exchange is present all along the protein backbone and the sign of $\Delta\omega$ cannot be determined by the HARD experiment (Chao and Byrd, 2016) we could not calculate the structure of the excited state(s).

Here, for the first time, we report the detailed characterization of the conformational dynamics of the dsRBDs, which suggests that the presence of similar μs-ms timescale motions in two dsRBDs. Further, it hints towards these motions as a general feature of dsRBDs. These conformational dynamics lead to the creation of a conformational pool for the dsRBDs that might allow it to interact with target dsRNAs in the cellular environment. This may further allow processing of the accurate substrate dsRNAs by the catalytic protein partners of dsRBDs. Identification and characterization of the dynamics at the μs-ms timescale shows conformational adaptability of the dsRBDs and is a step towards in understanding the mechanism of non-specific interaction between dsRBD and target dsRNAs.

Conclusions

The observations show the presence of conformational plasticity in two dsRBDs irrespective of differences in their primary sequences. The effect of different primary sequences was reflected in the ps-ns timescale dynamics of the two proteins. However, the similar R_{ex} rates measured by the extended model-free approach and the μs-ms timescale dynamics measured by the NMR relaxation dispersion method are present all along the backbone of the protein in addition to the faster μs timescale motions in the RNA-binding region. This conformational plasticity and the μs-ms timescale dynamics in two dsRBDs might be responsible for the adaptation required by the dsRBDs to target conformationally distinct dsRNAs present in the cellular pool.

bioRxiv preprint doi: https://doi.org/10.1101/797449; this version posted October 8, 2019. The copyright holder for this preprint (which was not certified by peer review) is the author/funder. All rights reserved. No reuse allowed without permission.

Author Contributions

J.C. and H.P. conceived the approaches to dynamically characterize the model dsRBDs and wrote the paper. H.P. performed all the experiments and the data analysis in active discussions with J.C.

Acknowledgements

Authors thank Prof. Jennifer Doudna (University of California, Berkeley) for the TRBP plasmids and Prof. Frederic H.T. Allain (ETH Zurich) for ADAR-plasmid. Authors also acknowledge High Field NMR facility at IISER-Pune (co-funded by DST-FIST and IISER Pune) and the High-Field NMR facility at IIT Bombay. This work was supported by funding from Indian Institute of Science, Education and Research, Pune; Department of Biotechnology, Govt. of India [No. BT/PR24185/BRB/10/1605/2017]; and extramural funding from the Science and Engineering Research Board (SERB), Govt. of India [EMR/2015/001966]. We acknowledge Dr. Radha Chauhan, Ms. Sangeeta Niranjan, and Ms. Bhawana Burdak for the help with measurement and analysis of the SEC-MALS data at NCCS, Pune. Authors also acknowledge Prof. Gianluigi Veglia (University of Minnesota, Minnesota) and Dr. Fa-An Chao (National Cancer Institute, Maryland) for active discussions while setting up HARD experiments and data analysis. Authors thank Dr. Arnab Mukherjee and Dr. T.S. Mahesh at IISER Pune for helpful discussion as Research Advisory Committee members for HP. Authors also thank Dr. Shilpy Sharma (Savitribai Phule Pune University, Pune) for active discussions during the data analysis and writing of the manuscript. HP is thankful to IISER Pune for the fellowship.

Declaration of interest

The authors declare no competing interest.

Supplementary Information

Supplementary Information (SI) available.

Methods Details

Protein Expression and Purification.

The plasmids containing the gene for TRBP2-dsRBD1 and dADAR-dsRBD1 were kindly provided by Prof. Jennifer Doudna (Noland, Ma and Doudna, 2011; Noland and Doudna, 2013) and Prof. Frederic Allain (Barraud *et al.*, 2012) respectively. The recombinant proteins – TRBP2-dsRBD1 and dADAR-

bioRxiv preprint doi: https://doi.org/10.1101/797449; this version posted October 8, 2019. The copyright holder for this preprint (which was not certified by peer review) is the author/funder. All rights reserved. No reuse allowed without permission.

dsRBD1 – were expressed and purified as described elsewhere (Barraud *et al.*, 2012; Paithankar *et al.*, 2018). For ^{15}N labeling, the protein was prepared by growing the cells in the M9 media containing $^{15}NH_4Cl$ (Cambridge Isotope Laboratories) as a sole source of nitrogen.

Circular Dichroism Spectroscopy.

All the Circular dichroism (CD) experiments were carried out on Jasco J-815 CD spectropolarimeter using a quartz rectangular cuvette of 2 mm path length. The bandwidth was set at 1 nm and the data was acquired with a scanning speed of 200 nm/min with an averaging time of 1 sec. The protein samples were exchanged with Buffer A (10 mM Sodium phosphate, 100 mM NaCl, 1 mM EDTA and 1 mM DTT) pH 6.4. The CD data was acquired on 20 μM of protein in the far-UV region from 200 to 250 nm in steps of 1 nm measured in temperature range from 10 to 80 °C at steps of 5 °C. An average of 3 scans was taken at each temperature. Protein was equilibrated for at least 10 min at a given temperature before starting the measurement. All CD spectra were baseline corrected by buffer.

The CD data thus obtained were smoothened using a five-point averaging method. The fraction folded (α) at each temperature was calculated as (Greenfield, 2006):

$$\boldsymbol{\alpha} = \frac{S_{obs} - S_U}{S_F - S_U} \qquad (1)$$

where, S_{obs}, S_U, S_F are the molar ellipticity at a given temperature, for the completely unfolded state and for the folded state, respectively. The thermodynamic parameters of the unfolding event were calculated by fitting CD data to Gibbs-Helmholtz equations (Greenfield, 2006):

$$\Delta G = \Delta H(1 - T/T_M) - \Delta C_P((1 - T/T_M) + T ln(T/T_M) \qquad (2)$$

$$K = \exp(-\Delta G/RT) \qquad (3)$$

$$\alpha = K/(1 + K) \qquad (4)$$

where, ΔH describes the enthalpy change, ΔC_P the heat capacity change, T_M is the temperature at mid-point of the unfolding transition, ΔG is the free energy of unfolding at Temperature T (Kelvin), K is the constant of folding at temperature T, and R is the gas constant (1.98 cal $K^{-1}mol^{-1}$).

Size Exclusion Chromatography – Multiple Angle Light Scattering.

SEC-MALS analysis of the purified proteins was performed on Superdex 75 10/300 GL column (GE Healthcare) using an Agilent HPLC system equipped with the 18-angle light scattering detector (Wyatt Dawn HELIOS II) and a refractive index detector (Wyatt Optilab T-rEX). The system was calibrated with a 100 μl injection volume of 30 μM Bovine Serum Albumin solution (ThermoScientific). 100 μl protein sample was injected (in duplicates) at a concentration of 459 μM and 1.1 mM for TRBP2-dsRBD1 and dADAR-dsRBD1, respectively. The molecular weights of the peaks were determined using Zimm model in ASTRA software version 6.1.7.17 (Wyatt Technologies).

NMR spectroscopy.

bioRxiv preprint doi: https://doi.org/10.1101/797449; this version posted October 8, 2019. The copyright holder for this preprint (which was not certified by peer review) is the author/funder. All rights reserved. No reuse allowed without permission.

All the NMR experiments were carried out on 1) Ascend™ Bruker 600 MHz NMR spectrometer equipped with quadruple-resonance ($^{1}H/^{15}N/^{13}C/^{31}P$) 5 mm Cryoprobe, X, Y, Z-gradients, and dual receiver operating; and 2) Ascend™ Bruker 750 MHz NMR spectrometer equipped with TXI probe, Z-gradient, and deuterium decoupling. All the NMR experiments were recorded at 25 °C. All the NMR spectra were processed using NMRPipe/NMRDraw (Delaglio *et al.*, 1995) and were analyzed using SPARKY (Lee, Tonelli and Markley, 2015). Representative ^{1}H-^{15}N-HSQC spectra for TRBP2-dsRBD1 and dADAR-dsRBD1 have been depicted in Figure S6.

Nuclear spin relaxation experiments were measured at two field strengths (an in-house 600 MHz NMR spectrometer and 750 MHz NMR spectrometer located at IIT Bombay) on a 1.8 mM ^{15}N-TRBP2-dsRBD1 sample and 0.69 mM ^{15}N-dADAR-dsRBD1 sample in Shigemi tubes. For TRBP2-dsRBD1, ^{15}N transverse relaxation rates (R_2) were measured with eight CPMG delays of 17, 34*, 51, 68, 85, 102, 136*, and 170 ms. ^{15}N longitudinal relaxation rates (R_1) were measured with ten inversion recovery delays of 10, 30, 50*, 100, 200, 300, 450, 600, 750*, and 900 ms. For dADAR-dsRBD1, seven CPMG delays of 17, 34, 68*, 102, 136, 170, and 204* ms and eight inversion recovery delays of 10, 30, 50*, 100, 200, 350, 500*, and 750 ms were used to measure R_2 and R_1 relaxation rates, respectively. Delays marked with an asterisk in both the experiments were measured in duplicate for estimation of errors in relaxation rates. Steady-state [^{1}H]-^{15}N heteronuclear nOe measurements were carried out with a ^{1}H saturation time of 3 s and a relaxation delay of 2 s for both the proteins. For the experiment without ^{1}H saturation, the relaxation delay of 5 s was used. All the nuclear spin relaxation experiments were measured in an interleaved fashion and with randomized order of delays.

^{15}N relaxation dispersion experiments were measured using constant time CPMG (Carr-Purcell-Meiboom-Gill) experiments (Tollinger *et al.*, 2001) at two static magnetic fields (600 MHz and 750 MHz). For TRBP2-dsRBD1, each relaxation dispersion profile was composed of 9 points with ν_{cpmg} values of 25, 50*, 100, 200, 350, 500, 650*, 800, and 1000 Hz at constant relaxation time, T_{relax}, of 40 ms. For dADAR-dsRBD1, relaxation dispersion profile was recorded with ν_{cpmg} of 50, 100, 150*, 200, 300, 450, 600*, 800 and 1000 Hz with T_{relax} of 20 ms. Duplicate points were measured for error analysis and have been marked with an asterisk.

Heteronuclear Adiabatic Relaxation Dispersion (HARD) experiments were performed at 600 MHz NMR spectrometer. A composite adiabatic pulse of 16 ms containing four hyperbolic secant family pulses of 4 ms each was used for spin-locking the ^{15}N magnetization in both $R_{1\rho}$ and $R_{2\rho}$ experiments, as described earlier (Mangia *et al.*, 2010; Traaseth *et al.*, 2012). Relaxation dispersion was created with adiabatic hyperbolic secant pulses with different stretching factors (n=1,2,4,6,8). As the stretching factor was increased from 1 to 8, the effective spin-lock field strength increased. Relaxation delays for adiabatic $R_{1\rho}$ and $R_{2\rho}$ experiments were varied by varying the number of composite pulses applied during evolution. The relaxation delays used were 0, 16, 32, 48 and 64 ms corresponding to

bioRxiv preprint doi: https://doi.org/10.1101/797449; this version posted October 8, 2019. The copyright holder for this preprint (which was not certified by peer review) is the author/funder. All rights reserved. No reuse allowed without permission.

the number of composite adiabatic pulses of 0, 1, 2, 3, 4. R_1 experiments were acquired in the same way as $R_{1\rho}$ and $R_{2\rho}$ experiments without using the adiabatic pulse during evolution. Relaxation delays used for the R_1 experiment were 16, 48, 96, 192, 320, and 480 ms. An inter-scan delay of 2.5 s and 3 s was used for TRBP2-dsRBD1 and dADAR-dsRBD1, respectively in all the above relaxation experiments.

NMR relaxation Data Analysis.

Relaxation rates in $R_1/R_2/R_{1\rho}/R_{2\rho}$ experiments were calculated by fitting the intensity data against relaxation delays to mono-exponential decays in Mathematica (Spyracopoulos, 2006). Errors in the relaxation rates were calculated as fit errors using a combination of duplicate delay and Monte Carlo simulations. [^{1}H]-^{15}N nOe values were obtained as a ratio of the intensity of respective peaks of the spectra recorded with and without saturation. Errors in nOe values were obtained by propagating the errors from RMSD values of baseline noise as obtained from Sparky.

Analysis of the ^{15}N-relaxation data (R_1, R_2, [^{1}H]-^{15}N nOe) recorded at two magnetic fields was done using the extended model-free formalism (Lipari and Szabo, 1982c, 1982a; Clore *et al.*, 1990) with the graphical user interface provided by the Relax v4.0.3 software (d'Auvergne, 2006; Bieri, d'Auvergne and Gooley, 2011). The ^{1}H-^{15}N dipole-dipole interaction and CSA values (-172 ppm) were included in calculations as per the default protocol. The distance between N and H was set as 1.02 Å. First, the local τ_m diffusion model was optimized with no global diffusion parameter defined. Diffusion tensor values for various diffusion models – sphere, spheroid, and ellipsoid – were calculated using the program quadric diffusion (Lee *et al.*, 1997) for data recorded at both the magnetic fields. Solution structure of TRBP2-dsRBD1 (Paithankar *et al.*, 2018) and dADAR-dsRBD1 (Barraud *et al.*, 2012) was used to optimize the diffusion tensor parameters. These diffusion tensor parameters were then used to calculate the model-free parameters from the ten model-free models and the best model for each residue was selected based on Akaike's Information Criteria. After the selection of these local models, diffusion tensor was further optimized with fixed local models. This was repeated until all the model-free parameters converged. The global diffusion model was then selected based on the chi-squared values obtained from optimized diffusion models. The error analysis for the selected model (global and local) was done using the Monte Carlo method.

For CPMG relaxation dispersion experiments, effective transverse relaxation rates at each CPMG frequency were extracted using the following equation (Loria, Berlow and Watt, 2008):

$$\boldsymbol{R_{2eff}} = \frac{\mathbf{1}}{T_{relax}} \mathbf{log}\left(\frac{I_0}{I_{cpmg}}\right) \qquad (5)$$

where, I_0 is the intensity of a peak in reference spectrum and I_{cpmg} is the intensity of the respective peak in the spectrum with CPMG field applied at a frequency ν_{cpmg}. The R_{2eff} rates thus obtained were plotted against the CPMG frequency ν_{cpmg}.

bioRxiv preprint doi: https://doi.org/10.1101/797449; this version posted October 8, 2019. The copyright holder for this preprint (which was not certified by peer review) is the author/funder. All rights reserved. No reuse allowed without permission.

For HARD experiments, the relaxation rates (R_1, $R_{1\rho}$, and $R_{2\rho}$) along with rotational correlation time calculated from the model-free analysis was used to fit the data to the time-dependent Bloch-McConnell equation assuming a two-site exchange model. The solution to the equation by using a geometric approximation method allowed to extract the dynamic parameters and the relaxation rates during the chemical exchange process as described in detail elsewhere (Chao and Byrd, 2016).

References

Acevedo, R. et al. (2016) 'Binding by TRBP-dsRBD2 Does Not Induce Bending of Double-Stranded RNA', Biophysj. Biophysical Society, 110(12), pp. 2610–2617. doi: 10.1016/j.bpj.2016.05.012.

Bailor, M. H., Sun, X. and Al-Hashimi, H. M. (2010) 'Topology links RNA secondary structure with global conformation, dynamics, and adaptation', Science, 327(5962), pp. 202–206. doi: 10.1126/science.1181085.

Barraud, P. et al. (2012) 'Solution structure of the N-terminal dsRBD of Drosophila ADAR and interaction studies with RNA', Biochimie. Elsevier Masson SAS, 94(7), pp. 1499–1509. doi: 10.1016/j.biochi.2011.12.017.

Bass, B. L. (2007) 'RNA Editing by Adenosine Deaminases That Act on RNA Brenda', Annual Review of Biochemistry, 71, pp. 817–846. doi: 10.1016/j.biotechadv.2011.08.021.Secreted.

Beach, H. et al. (2005) 'Conservation of μs−ms Enzyme Motions in the Apo- and Substrate-Mimicked State', Journal of the American Chemical Society. American Chemical Society, 127(25), pp. 9167–9176. doi: 10.1021/ja0514949.

Bieri, M., d'Auvergne, E. J. and Gooley, P. R. (2011) 'relaxGUI: a new software for fast and simple NMR relaxation data analysis and calculation of ps-ns and mus motion of proteins', J Biomol NMR, 50(2), pp. 147–155. doi: 10.1007/s10858-011-9509-1.

Boehr, D. D. et al. (2006) 'The Dynamic Energy Landscape of Dihydrofolate Reductase Catalysis', Science, 313(5793), pp. 1638 LP – 1642. doi: 10.1126/science.1130258.

Bycroft, M. et al. (1995) 'NMR solution structure of a dsRNA binding domain from Drosophila staufen protein reveals homology to the N-terminal domain of ribosomal protein S5.', The EMBO Journal. John Wiley & Sons, Ltd, 14(14), pp. 3563–3571. doi: 10.1002/j.1460-2075.1995.tb07362.x.

Chakrabarti, K. S. et al. (2017) 'Conformational Dynamics and Allostery in E2:E3 Interactions Drive Ubiquitination: gp78 and Ube2g2', Structure, 25(5), pp. 794-805.e5. doi: https://doi.org/10.1016/j.str.2017.03.016.

Chao, F. A. and Byrd, R. A. (2016) 'Geometric Approximation: A New Computational Approach To Characterize Protein Dynamics from NMR Adiabatic Relaxation Dispersion Experiments', J Am Chem Soc, 138(23), pp. 7337–7345. doi: 10.1021/jacs.6b02786.

Chiliveri, S. C. et al. (2017) 'DRB4 dsRBD1 drives dsRNA recognition in Arabidopsis thaliana tasi/siRNA pathway', Nucleic Acids Research, 45(14), pp. 8551–8563. doi: 10.1093/nar/gkx481.

bioRxiv preprint doi: https://doi.org/10.1101/797449; this version posted October 8, 2019. The copyright holder for this preprint (which was not certified by peer review) is the author/funder. All rights reserved. No reuse allowed without permission.

Clore, G. M. et al. (1990) 'Deviations from the simple two-parameter model-free approach to the interpretation of nitrogen-15 nuclear magnetic relaxation of proteins', Journal of the American Chemical Society, 112(12), pp. 4989–4991.

d'Auvergne, E. J. (2006) Protein dynamics□: a study of the model-free analysis of NMR relaxation data. University of Melbourne. Available at: http://repository.unimelb.edu.au/10187/2281 Connect to thesis.

Daniels, S. M. et al. (2009) 'Characterization of the TRBP domain required for Dicer interaction and function in RNA interference', BMC Molecular Biology, 10(38). doi: 10.1186/1471-2199-10-38.

Delaglio, F. et al. (1995) 'NMRPipe: a multidimensional spectral processing system based on UNIX pipes', J Biomol NMR, 6(3), pp. 277–293. Available at: https://www.ncbi.nlm.nih.gov/pubmed/8520220.

Eisenmesser, E. Z. et al. (2002) 'Enzyme Dynamics During Catalysis', Science, 295(5559), pp. 1520 LP – 1523. doi: 10.1126/science.1066176.

Fareh, M. et al. (2016) 'TRBP ensures efficient Dicer processing of precursor microRNA in RNA-crowded environments', Nature Communications. Nature Publishing Group, 7, pp. 1–11. doi: 10.1038/ncomms13694.

Fraser, J. S. et al. (2009) 'Hidden alternative structures of proline isomerase essential for catalysis ', Nature, 462(7273), pp. 669–673. doi: 10.1038/nature08615.

Fu, Y. et al. (2016) 'Splicing variants of ADAR2 and ADAR2-mediated RNA editing in glioma', Oncol Lett, 12(2), pp. 788–792. doi: 10.3892/ol.2016.4734.

Gaspari, Z. and Perczel, A. (2010) 'Protein Dynamics as Reported by NMR', in Annual Reports on NMR Spectroscopy. 1st edn. Acadamic Press, pp. 35–75. doi: 10.1016/S0066-4103(10)71002-4.

Gatignol, A. et al. (1991) 'Characterization of a human TAR RNA-binding protein that activates the HIV-1 LTR', Science, 251(5001), pp. 1597–1600.

Greenfield, N. J. (2006) 'Using circular dichroism collected as a function of temperature to determine the thermodynamics of protein unfolding and binding interactions', NATURE PROTOCOLS, 1(6), pp. 2527–2535. doi: 10.1038/nprot.2006.204.

Ha, M. and Kim, V. N. (2014) 'Regulation of microRNA biogenesis.', Nature reviews. Molecular cell biology. Nature Publishing Group, 15(8), pp. 509–24. doi: 10.1038/nrm3838.

Hartman, E. et al. (2013) 'Intrinsic Dynamics of an Extended Hydrophobic Core in the S . cerevisiae RNase III dsRBD Contributes to Recognition of Specific RNA Binding Sites', Journal of Molecular Biology. Elsevier Ltd, 425(3), pp. 546–562. doi: 10.1016/j.jmb.2012.11.025.

Heber, S. et al. (2019) 'Staufen2-mediated RNA recognition and localization requires combinatorial action of multiple domains', Nature Communications, 10(1), p. 1659. doi: 10.1038/s41467-019-09655-3.

Ishima, R. and Torchia, D. A. (2000) 'Protein dynamics from NMR', Nature Structural Biology. Nature America Inc., 7, p. 740. doi: 10.1038/78963.

bioRxiv preprint doi: https://doi.org/10.1101/797449; this version posted October 8, 2019. The copyright holder for this preprint (which was not certified by peer review) is the author/funder. All rights reserved. No reuse allowed without permission.

Jie, J., Löhr, F. and Barbar, E. (2017) 'Dynein Binding of Competitive Regulators Dynactin and NudE Involves Novel Interplay between Phosphorylation Site and Disordered Spliced Linkers', Structure, 25(3), pp. 421–433. doi: https://doi.org/10.1016/j.str.2017.01.003.

Kamba, K., Nagata, T. and Katahira, M. (2015) 'Catalytic Analysis of APOBEC3G Involving Real-Time NMR Spectroscopy Reveals Nucleic Acid Determinants for Deamination', PLOS ONE. Public Library of Science, 10(4), p. e0124142. Available at: https://doi.org/10.1371/journal.pone.0124142.

Kempf, J. G. and Loria, J. P. (2002) 'Protein dynamics from solution NMR', Cell Biochemistry and Biophysics, 37(3), pp. 187–211. doi: 10.1385/CBB:37:3:187.

Kharrat, A. et al. (1995) 'Structure of the dsRNA binding domain of E. coli RNase III.', The EMBO Journal. John Wiley & Sons, Ltd, 14(14), pp. 3572–3584. doi: 10.1002/j.1460-2075.1995.tb07363.x.

Kleckner, I. R. and Foster, M. P. (2011) 'An introduction to NMR-based approaches for measuring protein dynamics', Biochimica et Biophysica Acta - Proteins and Proteomics. Elsevier B.V., 1814(8), pp. 942–968. doi: 10.1016/j.bbapap.2010.10.012.

Koh, H. R. et al. (2013) 'ATP-independent diffusion of double-stranded RNA binding proteins', Proceedings of the National Academy of Sciences, 110(1), pp. 151–156. doi: 10.1073/pnas.1212917110.

Kovrigin, E. L. and Loria, J. P. (2006) 'Enzyme Dynamics along the Reaction Coordinate:□ Critical Role of a Conserved Residue', Biochemistry. American Chemical Society, 45(8), pp. 2636–2647. doi: 10.1021/bi0525066.

Lee, H. Y. and Doudna, J. A. (2012) 'TRBP alters human precursor microRNA processing in vitro', RNA, 18(11), pp. 2012–2019. doi: 10.1261/rna.035501.112.

Lee, L. K. et al. (1997) 'Rotational diffusion anisotropy of proteins from simultaneous analysis of 15N and 13C alpha nuclear spin relaxation', J Biomol NMR, 9(3), pp. 287–298.

Lee, W., Tonelli, M. and Markley, J. L. (2015) 'NMRFAM-SPARKY: enhanced software for biomolecular NMR spectroscopy', Bioinformatics, 31(8), pp. 1325–1327. doi: 10.1093/bioinformatics/btu830.

Lipari, G. and Szabo, A. (1982a) 'Analysis of Nmr Relaxation Data on Macromolecules Using the Model-Free Approach', Biophysical Journal, 37(2), pp. A380–A380.

Lipari, G. and Szabo, A. (1982b) 'Model-Free Approach to the Interpretation of Nuclear Magnetic-Resonance Relaxation in Macromolecules .1. Theory and Range of Validity', Journal of the American Chemical Society, 104(17), pp. 4546–4559. doi: DOI 10.1021/ja00381a009.

Lipari, G. and Szabo, A. (1982c) 'Model-Free Approach to the Interpretation of Nuclear Magnetic-Resonance Relaxation in Macromolecules .2. Analysis of Experimental Results', Journal of the American Chemical Society, 104(17), pp. 4559–4570. doi: DOI 10.1021/ja00381a010.

Loria, J. P., Berlow, R. B. and Watt, E. D. (2008) 'Characterization of enzyme motions by solution NMR relaxation dispersion', Acc Chem Res, 41(2), pp. 214–221. doi: 10.1021/ar700132n.

Mangia, S. et al. (2010) 'Probing slow protein dynamics by adiabatic R(1rho) and R(2rho) NMR

bioRxiv preprint doi: https://doi.org/10.1101/797449; this version posted October 8, 2019. The copyright holder for this preprint (which was not certified by peer review) is the author/funder. All rights reserved. No reuse allowed without permission.

experiments', J Am Chem Soc, 132(29), pp. 9979–9981. doi: 10.1021/ja1038787.

Masliah, G. et al. (2018) 'Structural basis of siRNA recognition by TRBP double□stranded RNA binding domains', The EMBO Journal, p. e97089. doi: 10.15252/embj.201797089.

Masliah, G., Barraud, P. and Allain, F. H. (2013) 'RNA recognition by double-stranded RNA binding domains: a matter of shape and sequence', Cell Mol Life Sci, 70(11), pp. 1875–1895. doi: 10.1007/s00018-012-1119-x.

Nanduri, S. et al. (2000) 'A dynamically tuned double-stranded RNA binding mechanism for the activation of antiviral kinase PKR', EMBO J, 19(20), pp. 5567–5574. doi: 10.1093/emboj/19.20.5567.

Noland, C. L. and Doudna, J. A. (2013) 'Multiple sensors ensure guide strand selection in human RNAi pathways.', RNA (New York, N.Y.), 19(5). doi: 10.1261/rna.037424.112.

Noland, C. L., Ma, E. and Doudna, J. A. (2011) 'siRNA Repositioning for Guide Strand Selection by Human Dicer Complexes', Molecular Cell. Elsevier Inc., 43(1), pp. 110–121. doi: 10.1016/j.molcel.2011.05.028.

Paithankar, H. et al. (2018) '1H, 13C and 15N resonance assignment of domain 1 of trans-activation response element (TAR) RNA binding protein isoform 1 (TRBP2) and its comparison with that of isoform 2 (TRBP1)', Biomolecular NMR Assignments, pp. 189–194. doi: 10.1007/s12104-018-9807-6.

Popovych, N. et al. (2006) 'Dynamically driven protein allostery', Nature Structural &Amp; Molecular Biology. Nature Publishing Group, 13, p. 831. Available at: https://doi.org/10.1038/nsmb1132.

Savva, Y. A., Rieder, L. E. and Reenan, R. A. (2012) 'The ADAR protein family', Genome Biol, 13(12), p. 252. doi: 10.1186/gb-2012-13-12-252.

Spyracopoulos, L. (2006) 'A suite of Mathematica notebooks for the analysis of protein main chain 15N NMR relaxation data', J Biomol NMR, 36(4), pp. 215–224. doi: 10.1007/s10858-006-9083-0.

Stefl, R. et al. (2010) 'The Solution Structure of the ADAR2 dsRBM-RNA Complex Reveals a Sequence-Specific Readout of the Minor Groove', Cell, 143(2), pp. 225–237. doi: 10.1016/j.cell.2010.09.026.

Stephens, O. M., Haudenschild, B. L. and Beal, P. A. (2004) 'The binding selectivity of ADAR2's dsRBMs contributes to RNA-editing selectivity', Chem Biol, 11(9), pp. 1239–1250. doi: 10.1016/j.chembiol.2004.06.009.

Tants, J. N. et al. (2017) 'Molecular basis for asymmetry sensing of siRNAs by the Drosophila Loqs-PD/Dcr-2 complex in RNA interference', Nucleic Acids Research, 45(21), pp. 12536–12550. doi: 10.1093/nar/gkx886.

Tollinger, M. et al. (2001) 'Slow dynamics in folded and unfolded states of an SH3 domain', J Am Chem Soc, 123(46), pp. 11341–11352.

Traaseth, N. J. et al. (2012) 'Heteronuclear Adiabatic Relaxation Dispersion (HARD) for quantitative analysis of conformational dynamics in proteins', J Magn Reson, 219, pp. 75–82. doi:

bioRxiv preprint doi: https://doi.org/10.1101/797449; this version posted October 8, 2019. The copyright holder for this preprint (which was not certified by peer review) is the author/funder. All rights reserved. No reuse allowed without permission.

10.1016/j.jmr.2012.03.024.

Tzeng, S.-R. and Kalodimos, C. G. (2009) 'Dynamic activation of an allosteric regulatory protein', Nature, 462(7271), pp. 368–372. doi: 10.1038/nature08560.

Wang, X. et al. (2011) 'Dynamic mechanisms for pre-miRNA binding and export by Exportin-5', Rna, 17(8), pp. 1511–1528. doi: 10.1261/rna.2732611.

Wostenberg, C. et al. (2012) 'The Role of Human Dicer-dsRBD in Processing Small Regulatory RNAs', PLoS ONE, 7(12). doi: 10.1371/journal.pone.0051829.

Wostenberg, C., Quarles, K. A. and Showalter, S. A. (2010) 'Dynamic origins of differential RNA binding function in two dsRBDs from the miRNA "Microprocessor" complex', Biochemistry, 49(50), pp. 10728–10736. doi: 10.1021/bi1015716.